CMS Physics Analysis Summary

Contact: cms-pag-conveners-heavyions@cern.ch 2018/05/15

Charged particle angular correlations in XeXe collision at $\sqrt{s_{NN}} = 5.44$ TeV

The CMS Collaboration

Abstract

Azimuthal correlations of charged particles in xenon-xenon collisions at $\sqrt{s_{\mathrm{NN}}} = 5.44$ TeV are studied using data collected by the CMS experiment at the CERN LHC. The v_2, v_3, and v_4 Fourier coefficients that characterize the azimuthal behavior are obtained using two-particle correlations, the scalar product method and the multiparticle cumulant method. Within a hydrodynamic picture, these methods have different sensitivities to non-flow and flow fluctuation effects. The system size dependence of the results is explored by taking ratios with comparable results found in PbPb collisions. Model calculations that include fluctuation effects are compared to the experimental results.

1 Introduction

At sufficiently high temperatures, lattice quantum chromodynamics predicts a transition from ordinary hadronic matter to a state of deconfined quarks and gluons, the so-called "quark gluon plasma" (QGP) [1]. One of the key features of the QGP is its anisotropic collective behavior. Pressure gradients that result from the initial spatial anisotropy of the collision overlap region transform into a momentum anisotropy for the emitted particles. The collectivity of the QGP was first studied in gold-gold collisions at the Relativistic Heavy Ion Collider (RHIC) [2–5]. Later, this behavior was observed in lead-lead (PbPb) collisions at the Large Hadron Collider (LHC) [6–8], as well as in collisions involving medium sized systems, such as the copper-copper system studied at RHIC [9, 10]. More recently, collective behavior similar to that observed in the heavier systems has also been found in high multiplicity collisions involving the asymmetric proton-lead (pPb) system, and has even been observed in high multiplicity proton-proton (pp) collisions [6–8]. These light system results raise the question of the extent and system size dependence of QGP formation. The current results for medium mass xenon-xenon (XeXe) collisions bridge the gap between the light (pp and pPb) and heavy (PbPb) systems previously studied at LHC energies.

Anisotropic flow can be characterize by a Fourier expansion [11–13],

$$\frac{2\pi}{N}\frac{dN}{d\phi} = 1 + \sum_{n=1}^{\infty} 2v_n \cos[n(\phi - \Psi_n)], \tag{1}$$

where $\frac{dN}{d\phi}$ is the hadronic azimuthal density, ϕ is the azimuthal angle, and Ψ_n is the n^{th}-order event-plane angle, which is defined as the direction of the maximum final-state particle density for the n^{th}-order harmonic. The magnitude of the azimuthal anisotropy is characterized by the Fourier coefficients, v_n. The second- and third-order Fourier coefficients are referred to as "elliptic" (v_2) and "triangular" (v_3) flow, respectively. The former reflects the lenticular shape of the collision overlap region, while the later is a consequence of the initial-state fluctuations in the positions of nucleons at the moment of impact [14]. These two harmonics are believed to largely reflect the initial-state geometry [15]. For $n \geq 4$ the flow harmonics are also strongly affected by the dynamics of the system expansion. Hence, studying both the lower and higher flow harmonics is important for understanding of the medium created in heavy ion collisions.

In discussing the flow harmonics it is possible to define several different reference geometries. The "reaction plane" is the plane defined by the collision impact parameter and the beam direction. The "participant plane" is defined by the semi-minor axis of the region spanned by the nucleons that undergo a primary interaction and the beam direction. The "event plane" is defined by the direction of maximum outgoing particle density and the beam direction. The measured anisotropies are expressed in terms of the event plane. Averaged over many events, the event-plane results are expected to be similar to those that would be obtained if it were possible to determine the actual participant plane. Event-by-event fluctuations in the spatial overlap geometry lead to analysis-dependent differences in the v_n values [16]. The fluctuations cause an increase in the deduced v_n values found using two-particle correlations and the scalar product method, as compared to the corresponding participant plane value, while the four-particle cumulant v_n results are decreased. For fluctuations that follow a two-dimensional Gaussian behavior, the flow harmonics based on more than four particles are expected to be the same as the four-particle results. Deviations from this constant behavior can be used to estimate the higher-order moments of the fluctuation distribution. Comparison of flow coefficients measured by different methods is therefore an important way to probe the initial-state fluctuations.

This analysis presents measurements of the charged particle collective flow in the XeXe collision system at the center-of-mass energy per nucleon pair of $\sqrt{s_{\mathrm{NN}}} = 5.44\,\mathrm{TeV}$. The v_2, v_3 and v_4 Fourier coefficients are obtained by the methods of two-particle correlations ($v_n\{2\}$), scalar products ($v_n\{SP\}$) and multiparticle cumulants ($v_n\{m\}$). The results are shown as a function of transverse momentum, p_{T}, for the pseudorapidity region $|\eta| < 2.4$, and cover a wide centrality range (0-70%). Also, spectrum weighted values for the flow harmonics over the range $0.3 < p_T < 3.0\,\mathrm{GeV}/c$ are presented. The measured values are compared to corresponding ones from PbPb collisions at $\sqrt{s_{\mathrm{NN}}} = 5.02\,\mathrm{TeV}$. Theoretical predictions are compared to the observed system size dependence of the flow harmonics. These results provide new information on the initial-state geometry and its fluctuations, as well as the system size dependence of the medium response.

2 The CMS detector

The central feature of the CMS apparatus is a superconducting solenoid of 6 m internal diameter, providing a magnetic field of 3.8 T. Within the solenoid volume are a silicon pixel and strip tracker, a lead tungstate crystal electromagnetic calorimeter (ECAL), and a brass and scintillator hadron calorimeter (HCAL), each composed of a barrel and two endcap sections. Forward calorimeters extend the pseudorapidity coverage provided by the barrel and endcap detectors. Muons are detected in gas-ionization chambers embedded in the steel flux-return yoke outside the solenoid. The forward hadron (HF) calorimeter uses steel as an absorber and quartz fibers as the sensitive material. The two halves of the HF are located 11.2 m from the interaction region, one on each end, and together they provide coverage in the range $3.0 < |\eta| < 5.2$. They also serve as luminosity monitors. The HF calorimeters are azimuthally subdivided into 20° modular wedges and further segmented to form $0.175 \times 10^\circ (\Delta\eta \times \Delta\phi)$ towers. The silicon tracker measures charged particles within the pseudorapidity range $|\eta| < 2.5$. It consists of 1856 silicon pixel and 15 148 silicon strip detector modules. For nonisolated particles of $1 < p_{\mathrm{T}} < 10\,\mathrm{GeV}$ and $|\eta| < 1.4$, the track resolutions are typically 1.5% in p_{T} and 25–90 (45–150) μm in the transverse (longitudinal) impact parameter [17]. A more detailed description of the CMS detector, together with a definition of the coordinate system used and the relevant kinematic variables, can be found in Ref. [18]. The detailed MC simulation of the CMS detector response is based on Geant4 [19].

3 Events and track selection

The analysis is done using data recorded by CMS during the LHC XeXe run in 2017, corresponding to a total integrated luminosity of $3\mu\mathrm{b}^{-1}$. During the XeXe runs, the events were taken with a minimum bias trigger, without prescaling. At the hardware level (Level-1), the trigger required at least one tower of the Forward Hadronic calorimeter (HF) to be above an ADC count threshold that was fixed to maximize efficiency while keeping the noise contamination low. Offline, an additional High Level Trigger (HLT) was applied that required a single pixel track. The average pileup fraction was 0.01 per event. Events are further selected offline by requiring at least 3 GeV of energy being detected in each of three HF calorimeter towers on both sides of the CMS detector. Events are also required to have a reconstructed primary vertex, containing at least two tracks, located within 15 cm of the nominal collision point along the beam axis and within 0.2 cm in the transverse direction. In addition, a standard beam-scraping filter is applied. For each event with more than 10 tracks, this filter requires at least 25% of the tracks satisfy the track quality criteria that are discussed in Ref. [17]. The impact parameter

significance of the tracks with respect to the primary vertex in both the beam direction and the transverse plane must be less than 3, while the relative transverse momentum uncertainty must be below 10%. Events are further characterized by their centrality, a measure of the degree of geometric overlap of the two colliding nuclei [20], with 0% centrality corresponding to full overlap. The event centrality is determined offline and is based on the total energy measured in the HF calorimeters. Only tracks with $|\eta| < 2.4$ and $p_{\mathrm{T}} > 0.3\,\mathrm{GeV}/c$ are used in the analysis.

4 Analysis

The analysis techniques used in this study are fully described in previous CMS publications. The two-particle correlation method is discussed in Refs. [21, 22], while the scalar product and multiparticle cumulant analyses follow the discussion in Ref. [23]. The two-particle correlation PbPb analysis used to obtain the comparison results is discussed in Ref. [24].

In the two-particle correlation analyses, a charged particle from one transverse momentum interval is used as a "trigger" particle, to be paired with all of the remaining charged particles from either the same or a different p_T interval, the "associated" particles. For a given trigger particle, the pairing is done in bins of pseudorapidity and azimuthal angle $(\Delta\eta, \Delta\phi)$. A similar mixed event pairing of particles is done to establish a background distribution. A Fourier analysis of the azimuthal correlation between the trigger and associated particles leads to $V_{n\Delta}$ coefficients, where $V_{n\Delta}(p_{\mathrm{T}}^{\mathrm{trig}}, p_{\mathrm{T}}^{\mathrm{assoc}}) = v_n(p_{\mathrm{T}}^{\mathrm{trig}})v_n(p_{\mathrm{T}}^{\mathrm{assoc}})$ if factorization is assumed. To avoid short-range, nonflow correlations, a pseudorapidity gap of $\Delta\eta > 2$ is required for the particle pairs.

The "scalar-product" event-plane measurements are based on "recentered" flow Q-vectors, with

$$\vec{Q}_n = \left(\sum_i^M w_i \cos\left(n\phi_i\right) - \left\langle \sum_i^M w_i \cos\left(n\phi_i\right) \right\rangle, \sum_i^M w_i \sin\left(n\phi_i\right) - \left\langle \sum_i^M w_i \sin\left(n\phi_i\right) \right\rangle \right). \quad (2)$$

Here, w_i is a weight for the i^{th} particle emitted at azimuthal angle ϕ_i. The summations are over the number of particles M within a given pseudorapidity range. The averages indicated by the angular brackets are taken over all events corresponding to a given (centrality, η range, p_{T} range) analysis bin. These averages correspond to the "recentering" operation and are needed to minimize detector acceptance effects. The flow coefficients, expressed in term of the Q-vectors, are given by

$$v_n\left\{\mathrm{SP}\right\} \equiv \frac{\left\langle Q_n Q_{nA}^* \right\rangle}{\sqrt{\frac{\left\langle Q_{nA} Q_{nB}^* \right\rangle \left\langle Q_{nA} Q_{nC}^* \right\rangle}{\left\langle Q_{nB} Q_{nC}^* \right\rangle}}}. \quad (3)$$

Here, the subscripts A, B, and C refer to three separate reference vectors established in different regions of pseudorapidity. The particles of interest are used to obtain the Q_n vector, which is correlated with the Q_{nA} reference vector. The Q_{nB} and Q_{nC} vectors are used to correct for the finite resolution of the numerator in Eq. 3. For the current measurement, particles of interest in the range $-0.8 < \eta < 0.0$ $(0.0 < \eta < 0.8)$ are correlated with unit weight with particles detected in the HF calorimeter with $3 < \eta < 5$ $(-5 < \eta < -3)$ and weighted by their transverse energy. The Q_{nB} vector corresponds to particles with $-0.5 < \eta < 0.5$ weighted by their p_{T} values.

The Q-cumulant method [25] is used in this analysis to obtain the 4-, 6-, and 8-particle n^{th}-order harmonic results by correlating unique combinations of 4, 6, and 8 particles within each event. The same method has been used in previous CMS analyses [23, 26, 27] using a generic

framework described in Ref. [28]. This framework allows for a track-by-track weighting to correct for detector acceptance effects.

5 Systematic uncertainties

Four different sources of systematic uncertainties are considered. To study the effect of the track selection on the final results, different track cuts are applied by varying limits for the impact parameter significance from 2 to 5, and the relative p_{T} error from 0.05 to 0.1. These variations are found to have a 1% influence for peripheral collisions, increasing to 10% for the most central collisions at the lowest p_{T} values. The effect of moving the primary vertex position along the beam axis is studied by comparing the results with events from the vertex position ranges $|z_{vtx}| < 3$ cm and $3 < |z_{vtx}| < 15$ cm to the default range of $|z_{vtx}| < 15$ cm. A 1% systematic uncertainty is attributed to this source. The systematic uncertainty resulting from the XeXe centrality calibration is estimated by changing the event selection efficiency by $\pm 3\%$. This uncertainty is largest for the most peripheral centrality bin, where it reaches a value of 3%. To explore the sensitivity of the results to the Monte Carlo simulations on which the efficiency calibrations are based, analyses based on the HYDJET event generator are done for generated tracks both before and after detector effects are taken into account. The results for the two cases differ by about 2% for most centrality ranges, but the difference increases to 10% for the most central events and the lowest transverse momentum. The observed differences are included as an analysis procedure systematic uncertainty. The uncertainties are calculated and assigned for each data point. The quoted numbers represent just the minimum and maximum across the centrality intervals used in the analysis. The total systematic uncertainty is obtained by combining the individual components in quadrature.

6 Results

Figure 1 shows the v_2 results, as a function of p_{T} and in eleven centrality bins, as measured with the different techniques. The two- and multi-particle correlation results are averaged over the pseudorapidity range with $|\eta| < 2.4$, while the SP results are based on tracks with $|\eta| < 0.8$. The elliptic flow values extracted from two-particle correlations show the same shape as found with the multi-particle correlations, but with higher magnitudes. The difference in the values based on the two methods can be directly related to event-by-event fluctuations of the v_2 coefficient. The v_2 magnitude increases with p_{T}, reaching a maximum around $3-4\,\mathrm{GeV}/c$, and then slowly decreases. The maximum shifts to a lower p_{T} value as the events become more peripheral. In the most peripheral events, the system is not of sufficient size to suppress a significant nonflow contribution resulting from jets, even for lower transverse momenta. In these very peripheral events, the $v_2\{2\}$ distribution becomes almost flat for $p_{\mathrm{T}} > 3.0\,\mathrm{GeV}/c$

The difference between the 2- and 4-particle results is even larger for the v_3, triangular flow coefficients, as shown in Fig. 2. For most centralities, the 4-particle results have no clear maximum and their p_{T} dependence is not as prominent as that found for the 2-particle and scalar product methods. This suggests a larger fluctuation component to triangular flow, as compared to elliptic flow, as would be expected if the v_3 correlations are dominated by initial-state fluctuations [14].

The v_4 results from the two-particle correlation and scalar product analyses are presented in Fig. 3. As also found for the v_2 and v_3 harmonics, the SP values are only slightly larger than the two-particle correlation results. While fluctuation effects are expected to have a similar influence on these two methods, as implemented the methods cover different effective pseu-

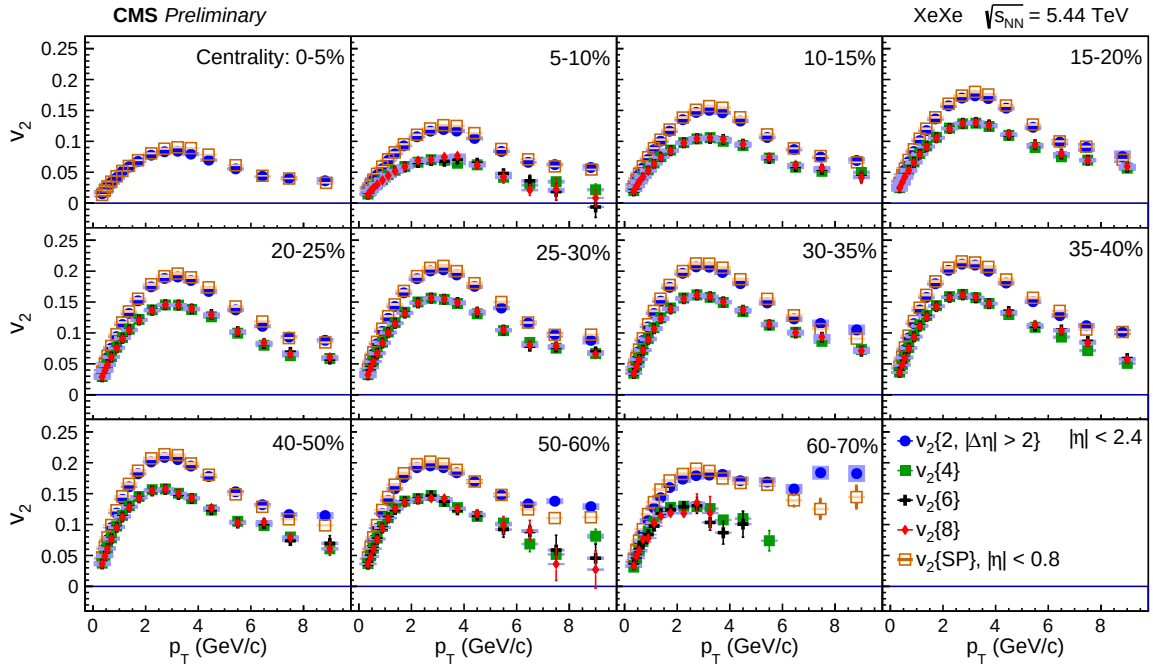

Figure 1: Elliptic flow coefficient, v_2, based on different analysis techniques, as a function of transverse momentum and in eleven centrality bins. The results for the 2- and multi-particle correlations correspond to the range $|\eta| < 2.4$, while the SP results are for $|\eta| < 0.8$. The shaded boxes represent systematic uncertainties.

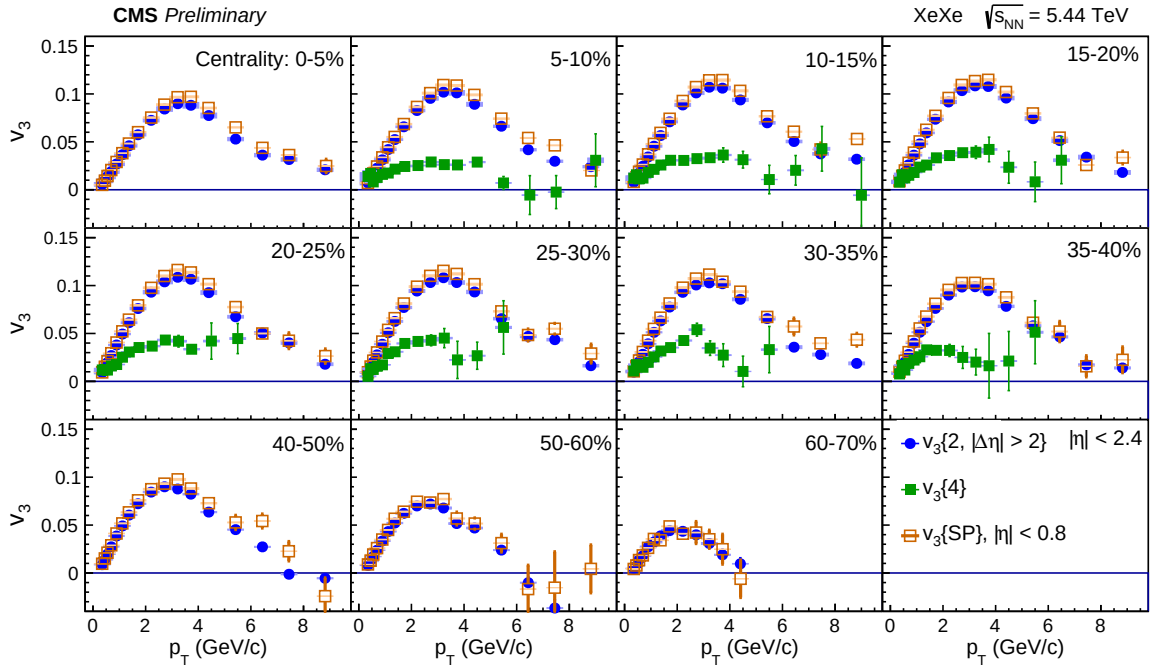

Figure 2: Triangular flow coefficients, v_3, based on the different analysis techniques, as a function of transverse momentum and in eleven centrality bins. The results for the 2- and multi-particle correlations correspond to the range $|\eta| < 2.4$, while the SP results are for $|\eta| < 0.8$. The shaded boxes represent systematic uncertainties.

dorapidity ranges. The similarity of the results suggests there is only a weak pseudorapidity dependence for all harmonics.

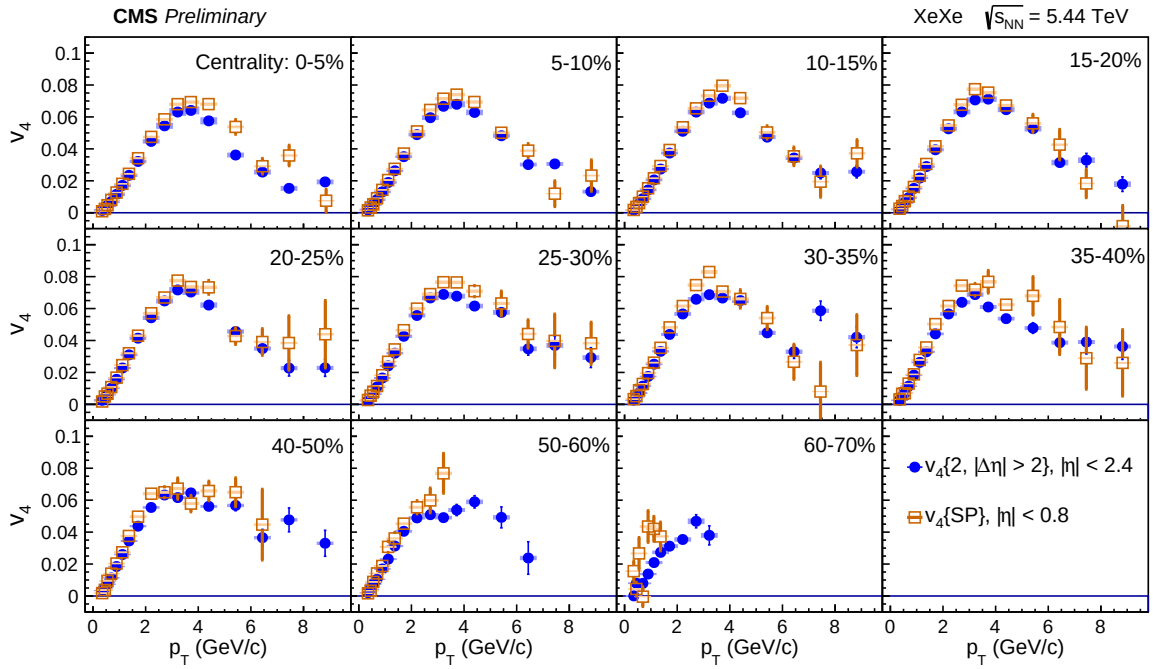

Figure 3: The v_4 coefficients, based on the different analysis techniques, as a function of transverse momentum and in eleven centrality bins. The results for the 2- and multi-particle correlations correspond to the range $|\eta| < 2.4$, while the SP results are for $|\eta| < 0.8$. The shaded boxes represent systematic uncertainties.

The spectrum-integrated single-particle anisotropy coefficients, as found using the different analysis methods, are presented in Fig. 4. The v_2 coefficients show a strong centrality dependence with a maximum value in the 40–50% centrality bin. The v_3 and v_4 coefficients change very weakly with centrality. Results based on multiparticle cumulants are below the $v_n\{2\}$ values, as expected. The predictions of the IP-Glasma + Music + UrQMD model are compared to the experimental $v_2\{2\}$ results. In this model, initial-state dynamics are described by impact parameter dependent, flowing Glasma gluon fields [29]. The subsequent hydrodynamic evolution is calculated with a MUSIC simulation and the simulation switches from a fluid-dynamical description to a transport description using the Ultrarelativistic Quantum Molecular Dynamics (UrQMD) transport model at the hadronization hypersurface [30]. The theory calculations are in good agreement with data for the v_2 and v_4 values. For the v_3 coefficient, the calculation gives slightly larger values than observed, with the difference increasing with increasing centrality.

Figure 5 shows the ratios $v_n\{4\}/v_n\{2\}$ for $n = 2$, and 3 and $v_2\{6\}/v_2\{4\}$. Theoretical predictions from hydrodynamic [31] and the IP-Glasma+Music+UrQMD models are compared to the experimental results. The hydrodynamic model starts the hydrodynamic evolution at a time $\tau = 0.6$ fm/c and has a shear viscosity to entropy ratio of $\eta/s = 0.047$. The $v_2\{4\}/v_2\{2\}$ ratio shows a strong centrality dependence, with the greatest deviation from unity corresponding to central events. The $v_3\{4\}/v_3\{2\}$ and $v_2\{6\}/v_2\{4\}$ ratios show little, if any, centrality dependence. The $v_2\{6\}/v_2\{4\}$ ratio is slightly below unity and suggests the existence of higher order corrections to a near-Gaussian distribution of the event-by-event flow fluctuations

The IP-Glasma+Music+UrQMD and hydrodynamic models give comparable agreement with

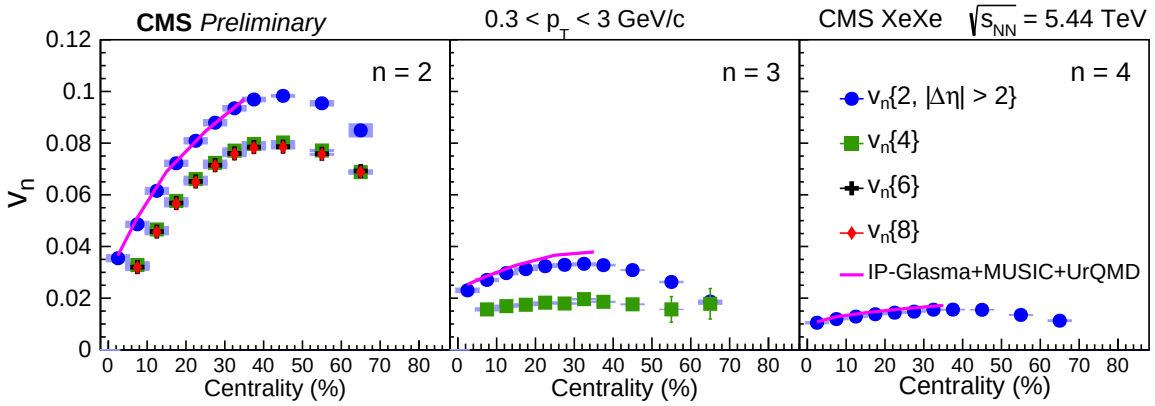

Figure 4: Centrality dependence of the spectrum-weighted v_2, v_3 and v_4 flow harmonics with $0.3 < p_T < 3.0\,\text{GeV}/c$. The v_2 results are shown for 2-, 4-, 6- and 8-particle correlations (left panel). The v_3 results are shown for 2- and 4-particle correlations (middle panel), while the v_4 values are presented for two-particle correlations technique, only. The shaded boxes represent systematic uncertainties.

data for the flow harmonic ratios. The hydrodynamic predictions are done considering both spherical and moderate prolate deformed xenon nuclei [32]. The later is more realistic and the absence of a significant difference comparing the two calculations suggests that fluctuations are not sensitive to the small deformation associated with the Xe nucleus.

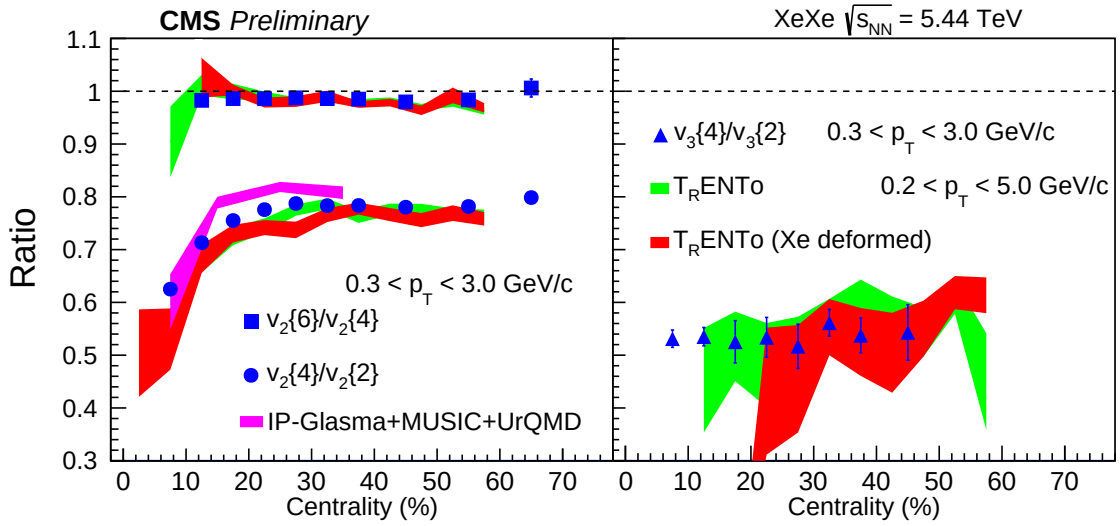

Figure 5: Centrality dependence of $v_2\{4\}/v_2\{2\}$, $v_2\{6\}/v_2\{4\}$ (left panel) and $v_3\{4\}/v_3\{2\}$ (right panel) ratios. Theoretical predictions based on the IP-Glasma + Music + UrQMD and the hydrodynamic model from Ref. [31] are compared to the data.

Since ideal hydrodynamics is scale invariant, the XeXe and PbPb results should have similar behavior [31]. However, initial-state fluctuations and viscous corrections can cause scale invariance braking. Fluctuations of the initial state are proportional to $A^{-1/2}$ and, therefore, one can expect a larger fluctuation component for XeXe collisions than for PbPb collisions [33]. However, the influence of the localized fluctuations will decrease with increasing viscosity. The viscosity is proportional to $A^{-1/3}$ [34] and is therefore also expected to be larger for XeXe collisions.

The v_2 coefficients, obtained by the two-particle correlations technique for XeXe collision at $\sqrt{s_{\mathrm{NN}}} = 5.44$ TeV are compared with corresponding PbPb data at 5.02 TeV as a function of transverse momentum in various centrality bins in Fig. 6. The v_2 values for the two systems show a similar dependence on p_{T}. However, the maximum value of the XeXe elliptic flow coefficient is only found to be greater than the corresponding PbPb value in the most central 0–5% bin. The v_3 coefficients for the two systems are compared in Fig. 7. For this harmonic, the PbPb results are only higher than the XeXe results for centralities above 35%. The v_4 coefficients for PbPb collisions are above the XeXe results for all centrality classes, as shown in Fig. 8.

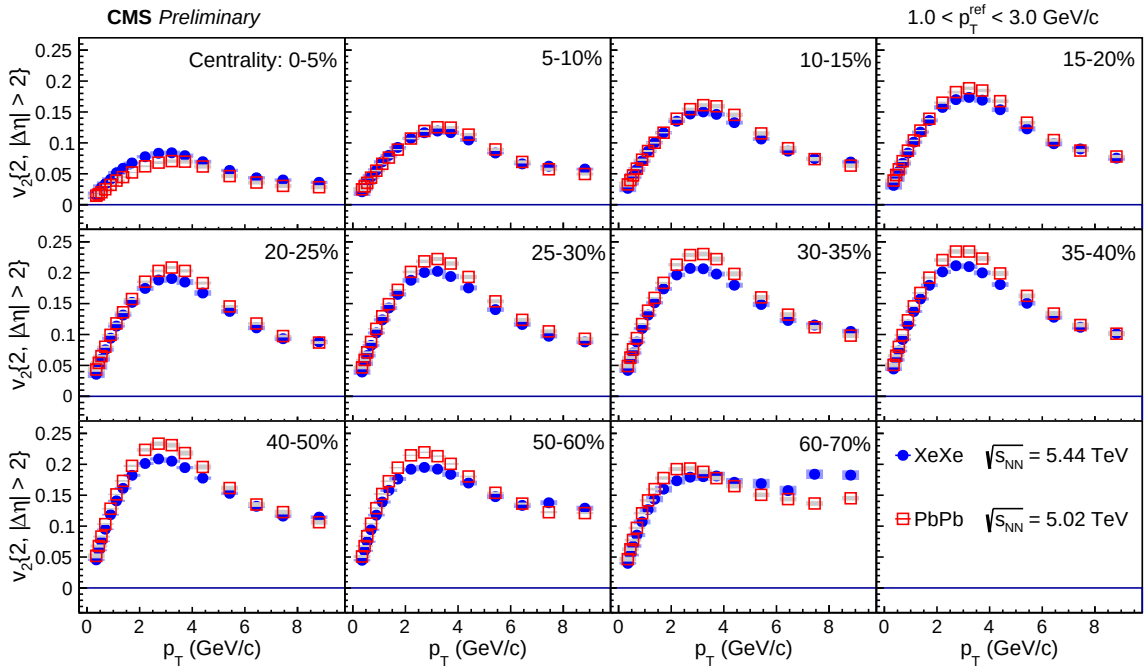

Figure 6: Comparison of v_2 results measured with two-particle correlations from two different systems, XeXe collisions at $\sqrt{s_{\mathrm{NN}}} = 5.44$ TeV and PbPb collisions at $\sqrt{s_{\mathrm{NN}}} = 5.02$ TeV, shown as a function of p_{T} in eleven centrality bins. The shaded boxes represent systematic uncertainties.

Figure 9 compares the spectrum-weighted v_2, v_3, and v_4 values with $0.3 < p_{\mathrm{T}} < 3.0\,\mathrm{GeV}/c$ for the XeXe and PbPb systems. The largest difference between the two systems is found for the v_2 coefficients corresponding to the most central events, where the XeXe results are larger by a factor of about 1.3. For centralities above 10%, the PbPb results become higher and the ratio has only a weak centrality dependence. For the v_3 and v_4 coefficients, the ratio $v_n[\mathrm{XeXe}]/v_n[\mathrm{PbPb}]$ decreases with centrality with an almost constant slope. The hydrodynamic model calculations of Ref. [31] are compared to the data. For all measured harmonics, the model values lie below the experimental results, with the greatest difference found for the v_4 coefficients. Based on the hydrodynamic model calculations, the quadrupole deformation of the colliding nuclei is expected to have the greatest influence for the v_2 values corresponding to the most central collisions. The observed increase in the ratio of $v_2[\mathrm{XeXe}]/v_2[\mathrm{PbPb}]$ for the most central events is consistent with this expectation.

For more peripheral events, multiplicity fluctuations in the forward region used to determine the event centrality can reduce the centrality resolution. This can lead to a XeXe centrality bias. Monte-Carlo studies using the HYDJET event generator indicate this bias could be as large as 5% in the 50–60% and 10% in the 60–70% centrality range for $v_n\{2\}$. For $v_n\{4\}$ the bias is less than 5% in the 60–70% centrality. For more central events the bias is found to be negligible.

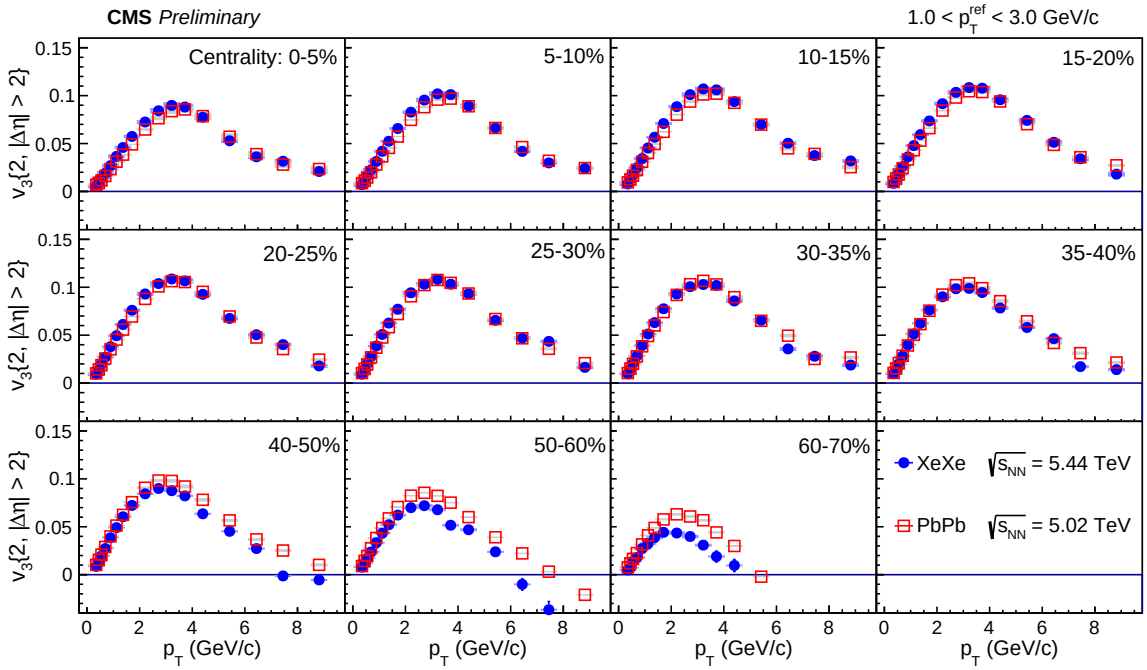

Figure 7: Comparison of v_3 results measured with two-particle correlations from two different systems, XeXe collisions at $\sqrt{s_{\mathrm{NN}}} = 5.44$ TeV and PbPb collisions at $\sqrt{s_{\mathrm{NN}}} = 5.02$ TeV shown as a function of p_{T} in eleven centrality bins. The shaded boxes represent systematic uncertainties.

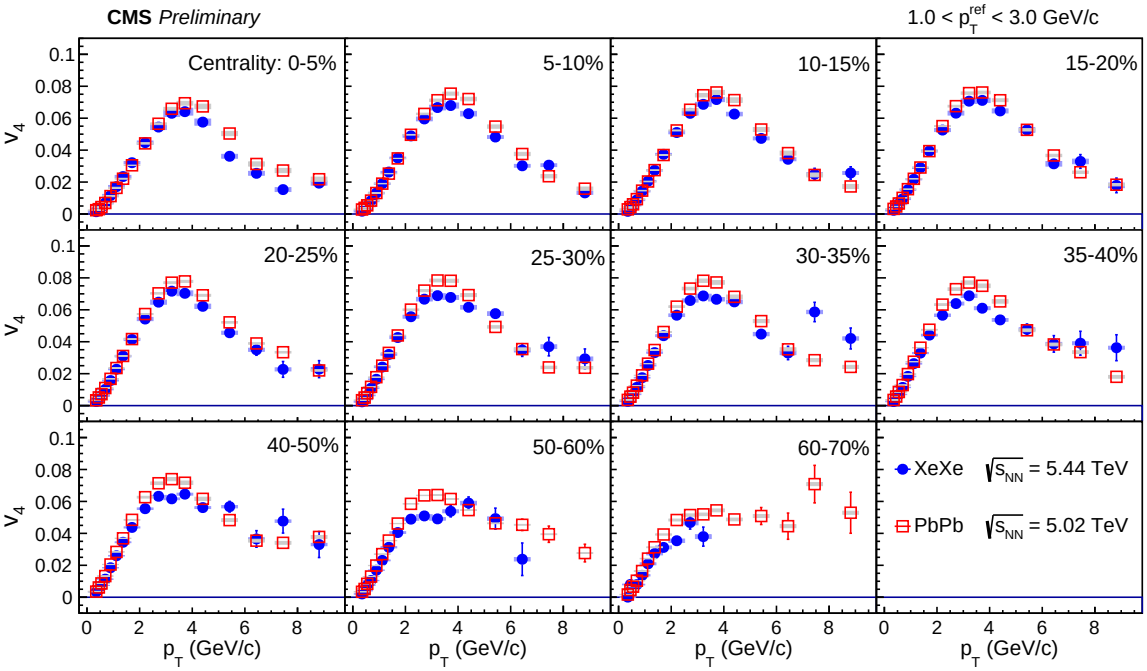

Figure 8: Comparison of v_4 results measured with two-particle correlations from two different systems, XeXe collisions at $\sqrt{s_{\mathrm{NN}}} = 5.44$ TeV and PbPb collisions at $\sqrt{s_{\mathrm{NN}}} = 5.02$ TeV, shown as a function of p_{T} in eleven centrality bins. The shaded boxes represent systematic uncertainties.

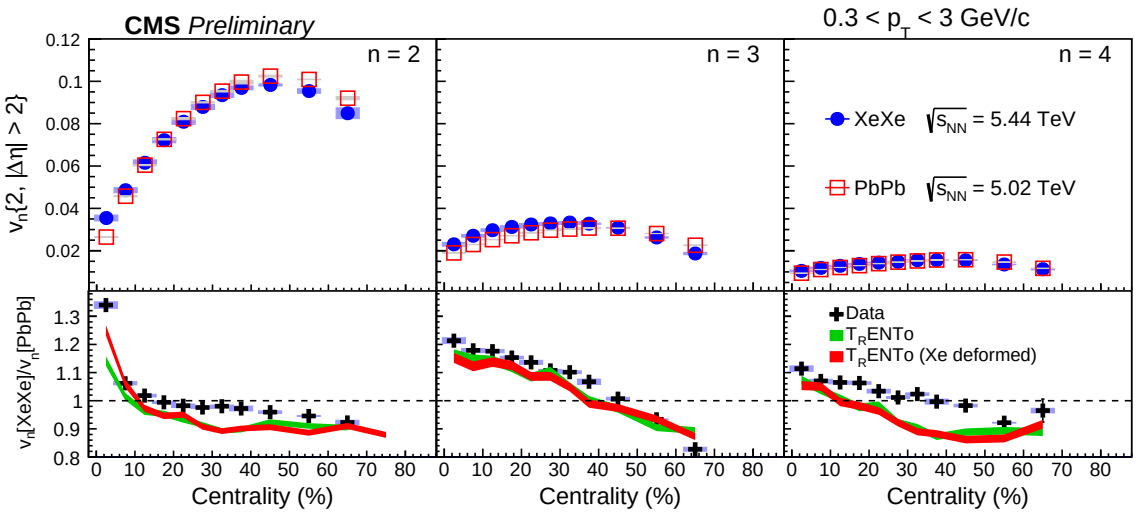

Figure 9: Centrality dependence of the spectrum-weighted v_2, v_3, and v_4 harmonic coefficient from two-particle correlations method with $0.3 < p_T < 3.0$ GeV/c for XeXe collisions at $\sqrt{s_{\rm NN}} = 5.44$ TeV and PbPb collisions at $\sqrt{s_{\rm NN}} = 5.02$ TeV. The lower panels show the ratio of the results for the two systems. Theoretical predictions from Ref. [31] are compared to the data. The shaded boxes represent systematic uncertainties.

Figure 10 shows the $p_{\rm T}$ dependent ratios of XeXe and PbPb harmonic coefficients. The ratios reach a maximum value between 1 and 2 GeV/c and then decrease to 6 GeV/c, at which point they start to increase. The increasing behavior above 6 GeV/c may be the consequence of back-to-back dijet correlations that can not be eliminated with the $|\Delta\eta| > 2$ cut.

7 Summary

In this note, the v_2, v_3 and v_4 azimuthal flow harmonics are shown for XeXe collisions at $\sqrt{s_{\rm NN}} = 5.44$ based on data obtained using the CMS detector. Three different analysis techniques, including two-particle correlations, the scalar product method, and the multiparticle cumulant method, are used to explore the fluctuation behavior through the different effect of flow fluctuations on each of these techniques. The harmonic coefficients are compared to those found with PbPb collisions at $\sqrt{s_{\rm NN}} = 5.02$ TeV to explore the influence of the system size. The magnitude of the v_2 coefficients for XeXe collisions are larger than found in PbPb collisions for the most central collisions. This is attributed to a larger fluctuation component in the lighter collision system. In more peripheral events, PbPb v_n coefficients are consistently greater than those found for XeXe collisions. This behavior is qualitatively consistent with expectations from hydrodynamic models. A clear ordering $v_2\{2\} > v_2\{4\} \approx v_2\{6\} \approx v_2\{8\}$ is observed, with a splitting of 2-3% for $v_2\{6\}/v_2\{4\}$. The $v_3\{4\}/v_3\{2\}$ ratio is found to be significantly smaller than the $v_2\{4\}/v_2\{2\}$ ratio for XeXe collisions, suggesting a dominant fluctuation component for the v_3 harmonic. Hydrodynamic models that consider the xenon nuclear deformation are better able to reproduce the centrality dependence of the $v_2[XeXe]/v_2[PbPb]$ ratio, although the deformation appears to have little effect on the overall fluctuation behavior. These measurements provide new tests on the hydrodynamics models and help to constrain hydrodynamical descriptions of the nuclear collisions.

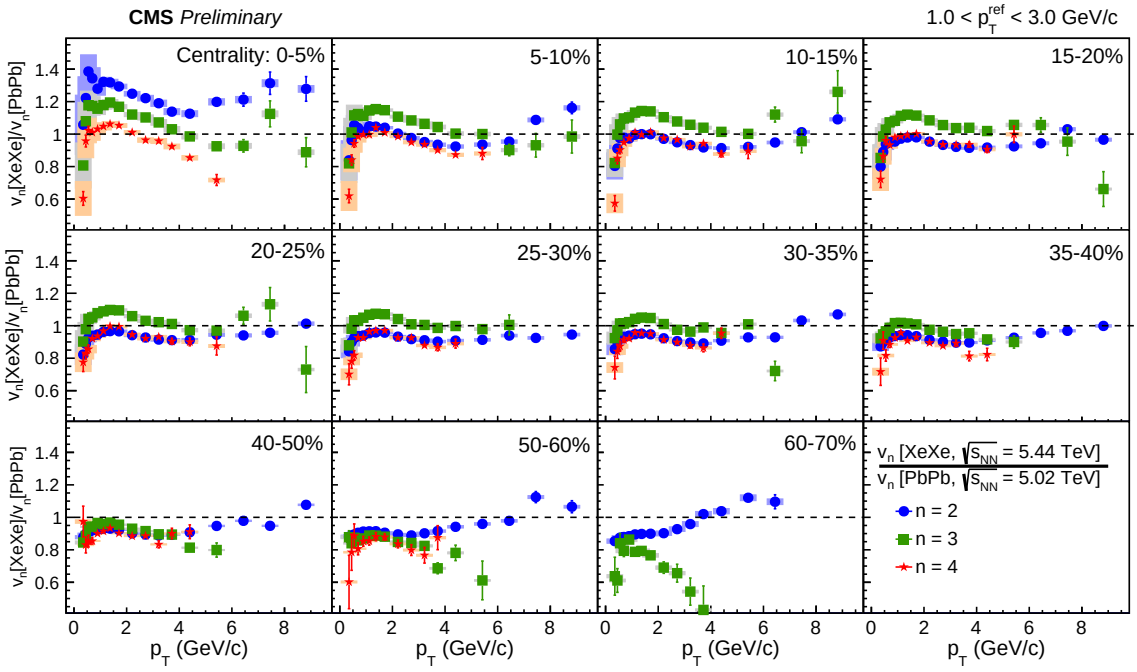

Figure 10: Ratio of the v_2, v_3, and v_4 harmonic coefficients from two-particle correlations for XeXe and PbPb collisions as a function of p_T in eleven centrality bins. The shaded boxes represent systematic uncertainties.

References

[1] F. Karsch, "Lattice QCD at High Temperature and Density", *Lect.Notes.Phys.* **583** (2002) 209–249, arXiv:hep-lat/0106019.

[2] BRAHAMS Collaboration, "Quark Gluon Plasma an Color Glass Condensate at RHIC? The perspective from the BRAHMS experiment", *Nucl. Phys. A* **757** (2005) 1, doi:10.1016/j.nuclphysa.2005.02.130, arXiv:nucl-ex/0410020.

[3] PHOBOS Collaboration, "The PHOBOS Perspective on Discoveries at RHIC", *Nucl. Phys. A* **757** (2005) 28, doi:10.1016/j.nuclphysa.2005.03.084, arXiv:nucl-ex/0410022.

[4] STAR Collaboration, "Experimental and Theoretical Challenges in the Search for the Quark Gluon Plasma: The STAR Collaboration's Critical Assessment of the Evidence from RHIC Collisions", *Nucl. Phys. A* **757** (2005) 102, doi:10.1016/j.nuclphysa.2005.03.085, arXiv:nucl-ex/0501009.

[5] PHENIX Collaboration, "Formation of dense partonic matter in relativistic nucleus-nucleus collisions at RHIC: Experimental evaluation by the PHENIX collaboration", *Nucl. Phys. A* **757** (2005) 184, doi:10.1016/j.nuclphysa.2005.03.086, arXiv:nucl-ex/0410003.

[6] CMS Collaboration, "Evidence for collectivity in pp collisions at the LHC", *Phys. Lett. B* **765** (2017) 193, doi:10.1016/j.physletb.2016.12.009, arXiv:1606.06198.

[7] CMS Collaboration, "Evidence for collective multi-particle correlations in pPb collisions", *Phys. Rev. Lett.* **115** (2015) 012301, doi:10.1103/PhysRevLett.115.012301, arXiv:1502.05382.

[8] ATLAS Collaboration, "Measurement of multi-particle azimuthal correlations with the subevent cumulant method in pp and p+pb collisions with the atlas detector at the lhc", *Phys. Rev. C* **97** (2018) 024904, doi:10.1103/PhysRevC.97.024904, arXiv:1708.03559.

[9] STAR Collaboration, "Charged and strange hadron elliptic flow in Cu+Cu collisions at 62.4 and 200 GeV", *Phys. Rev. C* **98** (2010) 044902, doi:10.1103/PhysRevC.81.044902, arXiv:1001.5052.

[10] PHENIX Collaboration, "Scaling properties of azimuthal anisotropy in Au+Au and Cu+Cu collisions at $\sqrt{s_{NN}} = 200$ GeV", *Phys. Rev. Lett.* **98** (2007) 162301, doi:10.1103/PhysRevLett.98.162301, arXiv:nucl-ex/0608033.

[11] J.-Y. Ollitrault, "Determination of the reaction plane in ultrarelativistic nuclear collisions", *Phys.Rev. D* **48** (1993) 1132, doi:10.1103/PhysRevD.48.1132, arXiv:hep-ph/9303247.

[12] S. Voloshin and Y. Zhang, "Flow study in relativistic nuclear collisions by Fourier expansion of azimuthal particle distributions", *Z. Phys. C* **70** (1994) 665–672, doi:10.1007/s002880050141, arXiv:hep-ph/9407282.

[13] A. M. Poskanzer and S. A. Voloshin, "Methods for analyzing anisotropic flow in relativistic nuclear collisions", *Phys. Rev. C* **58** (1998) 1671, doi:10.1103/PhysRevC.58.1671, arXiv:nucl-ex/9805001.

[14] B. Alver and G. Roland, "Collision geometry fluctuations and triangular flow in heavy-ion collisions", *Phys.Rev.* **C81** (2010) 054905, doi:10.1103/PhysRevC.81.054905, arXiv:1003.0194.

[15] Y. Li and J.-Y. Ollitrault, "v_4, v_5, v_6, v_7: nonlinear hydrodynamic response vs LHC data", *Phys.Lett. B* **744** (2015) 82–87, doi:10.1016/j.physletb.2015.03.040, arXiv:1502.02502.

[16] J.-Y. Ollitrault, A. M. Poskanzer, and S. A. Voloshin, "Effect of flow fluctuations and nonflow on elliptic flow methods", *Phys.Rev. C* **80** (2009) 014904, doi:10.1103/PhysRevC.80.014904, arXiv:0904.2315.

[17] CMS Collaboration, "Description and performance of track and primary-vertex reconstruction with the CMS tracker", *JINST* **9** (2014) P10009, doi:10.1088/1748-0221/9/10/P10009, arXiv:1405.6569.

[18] CMS Collaboration, "The CMS experiment at the CERN LHC", *JINST* **3** (2008) S08004, doi:10.1088/1748-0221/3/08/S08004.

[19] GEANT4 Collaboration, "Geant4 — a simulation toolkit", *Nucl. Instrum. Meth. A* **506** (2003) 250, doi:10.1016/S0168-9002(03)01368-8.

[20] M. L. Miller et al., "Glauber modeling in high energy nuclear collisions", *Ann. Rev. Nucl. Part. Sci.* **57** (2007) 205, doi:10.1146/annurev.nucl.57.090506.123020, arXiv:nucl-ex/0701025.

[21] CMS Collaboration, "Long-range and short-range dihadron angular correlations in central PbPb collisions at $\sqrt{s_{NN}} = 2.76$ TeV", *JHEP* **7** (2011) 076, doi:10.1007/JHEP07(2011)076, arXiv:1105.2438.

[22] CMS Collaboration, "Centrality dependence of dihadron correlations and azimuthal anisotropy harmonics in PbPb collisions at $\sqrt{s_{NN}} = 2.76$ TeV", *European Physics Journal C* **72** (2012) 10052, doi:10.1140/epjc/s10052-012-2012-3, arXiv:1201.3158.

[23] CMS Collaboration, "Pseudorapidity and transverse momentum dependence of flow harmonics in pPb and PbPb collisions", arXiv:1710.07864.

[24] CMS Collaboration, "Measurement of mixed higher order flow harmonics in PbPb collisions",.

[25] A. Bilandzic, R. Snellings, and S. Voloshin, "Flow analysis with cumulants: Direct calculations", *Phys.Rev.* **C83** (2011) 044913, doi:10.1103/PhysRevC.83.044913, arXiv:1010.0233.

[26] CMS Collaboration, "Evidence for Collective Multiparticle Correlations in p-Pb Collisions", *Phys. Rev. Lett.* **115** (2015), no. 1, 012301, doi:10.1103/PhysRevLett.115.012301, arXiv:1502.05382.

[27] CMS Collaboration, "Multiplicity and transverse momentum dependence of two- and four-particle correlations in pPb and PbPb collisions", *Phys. Lett.* **B724** (2013) 213–240, doi:10.1016/j.physletb.2013.06.028, arXiv:1305.0609.

[28] A. Bilandzic et al., "Generic framework for anisotropic flow analyses with multiparticle azimuthal correlations", *Phys.Rev.* **C89** (2014), no. 6, 064904, doi:10.1103/PhysRevC.89.064904, arXiv:1312.3572.

[29] B. Schenke and S. Schlichting, "3-D Glasma initial state for relativistic heavy ion collisions", *Phys.Rev.* **C94** (2016) 044907, doi:10.1103/PhysRevC.94.044907, arXiv:1605.07158.

[30] H. Petersen et al., "Fully integrated transport approach to heavy ion reactions with an intermediate hydrodynamic stage", *Phys.Rev.* **C78** (2008) 044901, doi:10.1103/PhysRevC.78.044901, arXiv:0806.1695.

[31] G. Giacalone, J. Noronha-Hostler, M. Luzum, and J.-Y. Ollitrault, "Hydrodynamic predictions for 5.44 TeV Xe+Xe collisions", *Unpublished* (2017) arXiv:1711.08499.

[32] P. Moller, S. A. J., T. Ichikawa, and H. Sagawa, "Nuclear ground-state masses and deformations: FRDM(2012)", doi:10.1016/j.adt.2015.10.002, arXiv:1508.06294.

[33] R. Bhalerao, M. Luzum, and J.-Y. Ollitrault, "Understanding anisotropy generated by fluctuations in heavy-ion collisions", *Phys.Rev.* **C84** (2011) 054901, doi:10.1103/PhysRevC.84.054901, arXiv:1107.5485.

[34] P. Romatschke and U. Romatschke, "Viscosity Information from Relativistic Nuclear Collisions: How Perfect is the Fluid Observed at RHIC?", *Phys.Rev. Lett.* **99** (2007) 172301, doi:10.1103/PhysRevLett.99.172301, arXiv:0706.1522.